Inorganic Chemistry

Article

pubs.acs.org/IC

Electrocatalytic Water Oxidation by a Water-Soluble Nickel Porphyrin Complex at Neutral pH with Low Overpotential

Yongzhen Han,[†] Yizhen Wu,[†] Wenzhen Lai,*[,†] and Rui Cao*[,†,‡]

[†]Department of Chemistry, Renmin University of China, Beijing 100872, China

[‡]School of Chemistry and Chemical Engineering, Shaanxi Normal University, Xi'an 710119, China

Supporting Information

ABSTRACT: The water-soluble cationic nickel(II) complex of *meso*-tetrakis(4-*N*-methylpyridyl)porphyrin (**1**) can electrocatalyze water oxidation to O_2 in neutral aqueous solution (pH 7.0) with the onset of the catalytic wave appearing at ∼1.0 V (vs NHE). The homogeneous catalysis with **1** was verified. Catalyst **1** exhibited water oxidation activity in a pH range 2.0−8.0 and had a strict linear dependence of catalytic current on its concentration. After 10 h of constant potential electrolysis at 1.32 V (vs NHE), a negligible difference of the solution was observed by UV−vis. In addition, inspection of the working electrode by electrochemistry, scanning electron microscope (SEM), and energy dispersive X-ray spectroscopy (EDX) showed no sign of deposition of NiO_x films. These results strongly argued that **1** is a real molecular electrocatalyst for water oxidation. The turnover frequency (TOF) for this process was 0.67 s^{-1} at 20 °C. On the basis of results from the kinetic isotope effect (KIE) and inhibition experiments, electrochemical studies in various buffer solutions with different anions and pHs, and DFT calculations, a catalytic cycle of **1** for water oxidation via a formally Ni(IV) species was proposed.

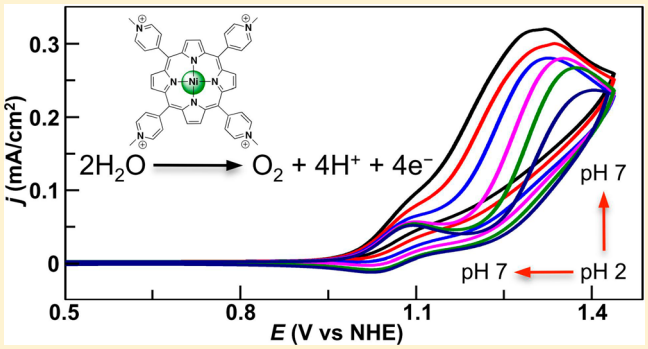

INTRODUCTION

Catalytic water oxidation is a subject of fundamental interest and significance because it is the half reaction to split water and is the key step in natural and artificial photosynthesis to convert and store solar energy.[1−9] As water oxidation that produces O_2 is challenging in both thermodynamic and kinetic aspects, the development of catalysts for oxygen evolution reaction (OER) that operate with low energy cost and with high efficiency and stability has attracted extensive interest.[10−13] Recent progress in homogeneous and heterogeneous OER catalysts has led to the discovery of active transition metals, including Ru,[14−20] Ir,[21−25] V,[26] Mn,[27] Fe,[28−31] Co,[8,13,32−36] and Cu.[11,37−42] Among these systems, mononuclear catalysts consisting of earth-abundant metals have many advantages, including low cost and easy syntheses, controllable redox features, and simple assemblies to other devices.[43−45] However, OER catalysts of first-row transition metals usually require relatively large overpotential to initiate water oxidation even in basic media,[11,34,37−40] and few have been shown to have low overpotential.[46] Therefore, improvements in catalysts to lower the energy inputs for OER are still needed.

Nickel is a first-row transition metal and has received particular interest for water oxidation because of its diverse redox properties and the strong oxidizing power of its high valence states. NiO_x and $Ni(OH)_2$ have been shown to be highly active for electrocatalytic water oxidation,[10,47−50] yet Ni-based molecular OER catalysts are much less explored. Recently, a macrocyclic Ni(II) amine complex was reported as the first molecular catalyst for water oxidation during the preparation of our Article.[51] However, more evidence is required to confirm the homogeneous nature of this catalysis, as macrocyclic Ni(II) amine complexes of this kind have already been proven to decompose and thus to form anodic deposition as active NiO_x films for water oxidation.[48]

Metalloporphyrins have been studied as electrocatalysts for the reduction of oxygen and proton,[52−56] but examples for the oxidation of water are rare. Recently, Wang and Groves reported on a series of water-soluble Co porphyrin catalysts for water oxidation at neutral pH with high efficiency and stability.[13] The use of cationic porphyrins inspired us to examine the catalytic performance of Ni analogues. We rationalized that the redox potential of high-valent Ni atoms is considerably higher than that of Co in the same valence state, which should be favored for the oxidation of water. Herein, we report a water-soluble cationic Ni(II) porphyrin **1** that functions as a single-site electrocatalyst for water oxidation in neutral aqueous solution with low overpotential. A combination of experiments and techniques, including pH-dependence and control experiments, KIE measurements, buffer anion and acetonitrile inhibition effects, electrochemistry, and spectroscopic and surface analysis, leads to a strong argument that

Received: April 24, 2015
Published: May 18, 2015

DOI: 10.1021/acs.inorgchem.5b00924
Inorg. Chem. 2015, 54, 5604−5613

catalyst **1** has homogeneous catalysis features for water oxidation. On the basis of results from a series of electrochemical studies and theoretical calculations, a catalytic cycle of **1** for water oxidation is proposed, in which a two-electron oxidized **1** is considered to be the catalytic active species to oxidize water.

RESULTS AND DISCUSSION

Synthesis and Characterization. Water-soluble nickel(II) porphyrin complex **1** (Figure 1) was prepared as hexafluorophosphate $\mathbf{1}(PF_6)_4$ and triflate $\mathbf{1}(OTf)_4$ salts. Crystals of both salts were obtained and used for characterization. Crystals of $\mathbf{1}(OTf)_4$ were used in all electrochemical and catalytic experiments due to its better solubility. Two Soret bands of **1** in water indicated an equilibrium of Ni atoms with and without axial aqua ligands[57] (Supporting Information Figure S1). The high-resolution mass spectrum showed an ion at a mass-to-charge ratio of 512.0845 (Supporting Information Figure S2), matching the calculated value of 512.0850 for the divalent ion $[\mathbf{1}(PF_6)_2]^{2+}$ with the expected isotopic distribution (0.5 unit separation between each peak). In the X-ray structures of $\mathbf{1}(OTf)_4$ and $\mathbf{1}(PF_6)_4$ (Supporting Information Figure S4), the two cationic Ni porphyrin units matched: each Ni atom has a four-coordinate square-planar geometry and is located perfectly at the center of the porphyrin ring. All four counteranions were successfully located in the X-ray structure of $\mathbf{1}(OTf)_4$ and $\mathbf{1}(PF_6)_4$. This result suggested the Ni(II) oxidation state. Complex **1** was further characterized by NMR spectroscopy. Consistent with its C_4 symmetry, there are four sharp signals in ^{1}H NMR (Supporting Information Figure S3). The peaks shown in this spectrum are sharp and clean and have the expected chemical shifts for a diamagnetic porphyrin species. This result was consistent with the d^8 Ni(II) electronic structure and indicated that the demetalation of Ni(II) porphyrin did not take place, as such a process would result in free porphyrin ligands and paramagnetic Ni(II) ions.

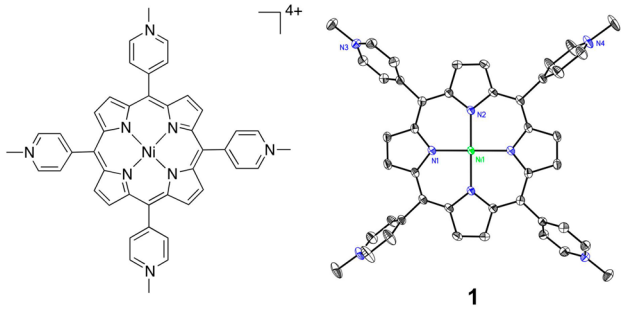

Figure 1. (Left) Molecular structure of Ni(II) porphyrin **1**. (Right) Thermal ellipsoid plot of the X-ray structure of **1** (50% probability). Hydrogen atoms and counteranions are omitted for clarity.

Electrochemical Water Oxidation. The cyclic voltammogram (CV) of 0.50 mM **1** in 0.10 M pH 7.0 phosphate buffer exhibited a pronounced catalytic activity, which was absent in CVs of buffer-only solutions (Figure 2a). The onset for this catalytic wave appeared at ~1.0 V versus the normal hydrogen electrode (NHE, all potentials reported in this paper are referenced to NHE). This value is smaller than that observed for its Co porphyrin analogue by ~200 mV,[13] and is even smaller than that for the biomimetic Cu catalyst recently reported by Lin and co-workers.[40] This feature is significant to meet the requirement for an OER catalyst to operate with low

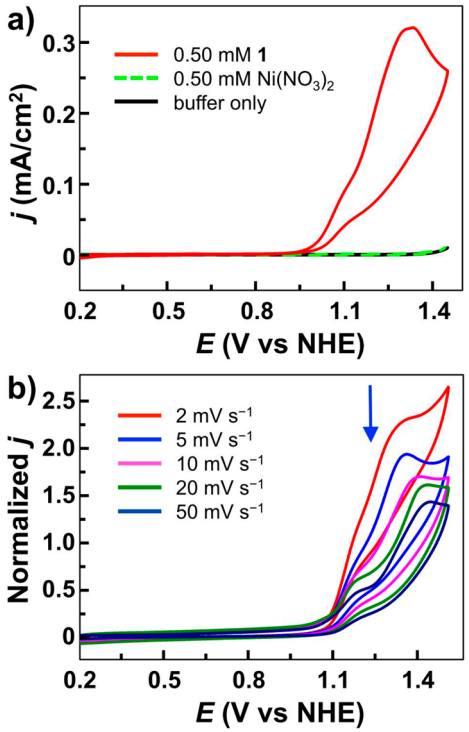

Figure 2. (a) CVs of **1**, $Ni(NO_3)_2$, and buffer-only solution at 50 mV s^{-1} scan rate. (b) Normalized CVs of 0.50 mM **1** at different scan rates in mA cm^{-2} $V^{-1/2}$ $s^{1/2}$. Conditions: ITO working electrode (S = 0.25 cm^{-2}), 0.10 M pH 7.0 phosphate buffer, 20 °C.

energy cost. It is necessary to point out that a shoulder anodic wave existed at 1.07 V, which corresponded to the one-electron redox couple of $[Por^{\bullet+}–Ni^{II}]^{5+}/[Por–Ni^{II}]^{4+}$ (see below). The normalized catalytic current ($i_{cat}/\nu^{1/2}$) decreased with increasing scan rates (Figure 2b), suggesting a catalytic process with a chemical rate-limiting step, which is likely O–O bond formation in this system (see below).[13,39]

In 20 successive CV cycles of **1**, no increase of catalytic current was observed (Supporting Information Figure S6), and the working electrode after 20 CV scans displayed no catalytic current in a buffer-only solution (Figure 3d). Importantly, 0.50 mM of $Ni(NO_3)_2$ under identical conditions showed no catalysis up to 1.45 V (Figure 2a). At higher potentials, the CV of free Ni(II) ions in 0.10 M pH 7.0 phosphate buffer displayed a crossover and a pronounced catalytic wave (Supporting Information Figure S5), which is indicative of the formation of active NiO_x films on the electrode. The onset potential for this catalytic wave was 1.60 V. This value is 600 mV larger than the onset with complex **1**. These results suggested that the observed catalytic activity of **1** was not caused by NiO_x films or free Ni(II) ions that may possibly be formed during catalysis.

Constant potential electrolysis (CPE) of **1** was carried out at 1.32 V in 0.1 M pH 7.0 phosphate buffer solution in a three-compartment gastight electrochemical cell with a Schlenk connection on each compartment. The evolved O_2 was analyzed by using a calibrated Ocean Optics FOXY probe (Model NeoFox), which was immersed into the solution having the ITO working electrode (Supporting Information Figure S19, details are described in Experimental Section). During 10 h of CPE, substantial current maintained with no current increase (Figure 3a). Faradaic efficiency of >90% for O_2

DOI: 10.1021/acs.inorgchem.5b00924
Inorg. Chem. 2015, 54, 5604–5613

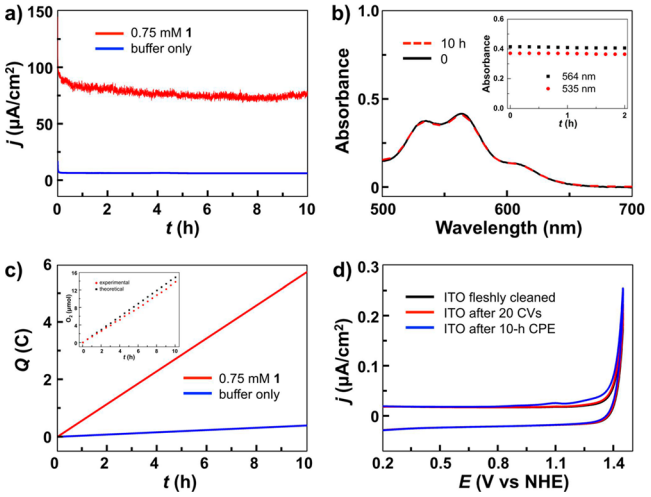

Figure 3. (a) Catalytic currents in CPE with and without **1** in 0.10 M pH 7.0 phosphate buffer at 1.32 V. (b) UV–vis spectra of **1** before and after 10 h of CPE. Insert: Plots of the absorption at 535 and 564 nm as a function of time during CPE. (c) The electric charge curve with and without **1** during 10 h of CPE. Insert: Detection of evolved O_2 during CPE and the theoretical amount of O_2 produced. (d) CVs of a freshly cleaned ITO electrode, an ITO after successive 20 CV cycles with **1**, and an ITO after 10 h of CPE with **1** in 0.10 M pH 7.0 phosphate buffer. Scan rate is 50 mV s^{-1}.

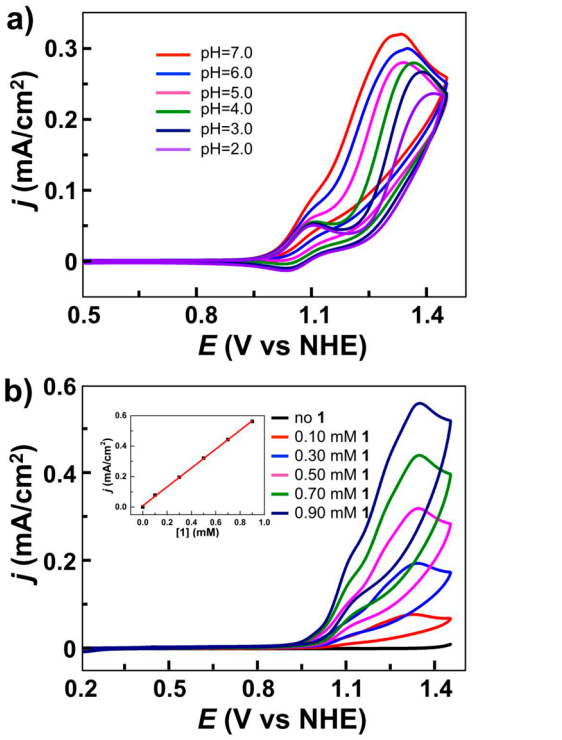

Figure 4. (a) CVs of 0.5 mM **1** in 0.10 M pH 2.0–7.0 phosphate buffers. (b) CVs of different concentrations of **1** in 0.10 M pH 7.0 phosphate buffer. Insert: Plot of catalytic current at E = 1.32 V vs [**1**]. Conditions: ITO working electrode, scan rate 50 mV s^{-1}, 20 °C.

evolution was obtained (Figure 3c and Supporting Information Figure S7).

As shown in Figure 3b and Supporting Information Figure S8, the UV–vis spectra of the aqueous solution of **1** during and after electrolysis showed negligible change throughout the CPE, which strongly argued for the molecular nature of this catalysis and the catalyst stability under turnover conditions for water oxidation. In addition, Tyndall scattering analysis of the aqueous solution of **1** after CPE revealed that no NiO_x particles were formed (Supporting Information Figure S9). Graphene oxide was used as a comparison because its aqueous solution has a similar color and has apparent Tyndall scattering effect. After 10 h of CPE, the ITO working electrode was removed from the solution of **1** and gently washed with deionized water, and was reexamined in a buffer-only solution. The CV of this ITO electrode displayed no catalytic current (Figure 3d). The surface morphology and composition of this ITO electrode were further inspected by SEM and EDX (Supporting Information Figures S10 and S11), which all clearly excluded the formation of any heterogeneous Ni phase on the working electrode.

Significantly, **1** was catalytically active in the pH range 2.0–8.0 (Figure 4a and Supporting Information Figure S13a). This result strongly argues against NiO_x materials that may possibly be generated from decomposed **1** acting as the real catalyst for water oxidation, as such species are unstable in acidic solutions.[32] In contrast to CVs of **1** in acidic and neutral solutions, when the pH was more than 9.0, another catalytic process appeared (Supporting Information Figure S13). For example, successive CV cycles of **1** in a pH 12.0 phosphate buffer exhibited a continuous increase of the catalytic current as well as the anodic current at ~0.78 V and cathodic current at ~0.67 V (Supporting Information Figure S15a), implying the formation and the deposition of active NiO_x films on the ITO electrode.[10,48,49] After 20 CV scans at pH 12.0, this working electrode displayed catalytic current in a buffer-only solution at pH 12.0, and this current retained over hundreds of CV scans at this pH (Supporting Information Figure S15b). However, if this NiO_x-deposited working electrode was examined in a neutral phosphate buffer, the catalytic current disappeared stepwise over several CV scans (Supporting Information Figure S15c). Similar electrochemical behaviors were observed in phosphate buffer solutions with pH > 9.0, and Supporting Information Figure S14 showed another example at pH 10.5. These results suggested that NiO_x was unstable by acting as the OER catalyst at neutral pH, which is consistent with the factor that NiO_x materials typically catalyze water oxidation in basic solutions.[10,48,49] In addition, the catalytic current had a strict linear dependence on the concentration of **1** (Figure 4b), which suggested that it is a single-site, molecular catalysis according to eq 1.

$$i_{cat} = n_{cat}FAc_{cat}\sqrt{k_{cat}D_{cat}} \quad (1)$$

Here, n_{cat} = 4 is the number of electrons for water oxidation to produce O_2, F is the Faraday constant, A is the electrode surface area, c_{cat} is the concentration of catalyst, k_{cat} is the apparent first-order rate constant, and D_{cat} is the diffusion coefficient of the catalyst (D_{cat} = 2.33 × 10^{-10} m^2 s^{-1} was calculated in sulfate solution at 20 °C according to eq 2 and Figure 5b, see below).

Mechanism Studies. In order to get more insights into the water oxidation mechanism, we examined the electrochemical behaviors of **1** in aqueous solution with different electrolytes. Unlike in phosphate buffer, the CV of **1** in 0.10 M sulfate solution showed no apparent catalytic current up to 1.35 V but displayed two oxidation waves at $E_{1/2}$ = 1.07 V and E_{pa} = 1.29 V (Figure 5a), which were assigned to the two one-electron oxidation processes of **1**. We rationalized that, in comparison to phosphate, sulfate is a much weaker base to assist O–O bond

DOI: 10.1021/acs.inorgchem.5b00924
Inorg. Chem. 2015, 54, 5604–5613

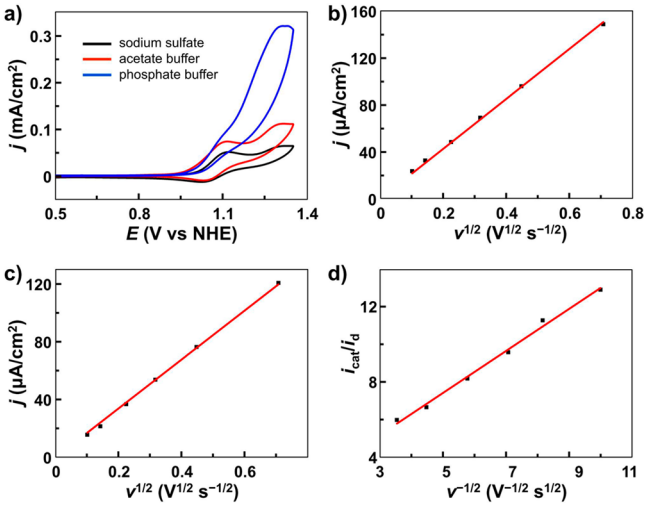

Figure 5. (a) CVs of **1** in 0.10 M various anion solutions with a scan rate of 50 mV s^{-1}. Dependence of the (b) first and (c) second oxidation peak current of **1** recorded in sulfate solution on the square root of scan rates. The peak currents of the first (in the absence of catalysis) and the second oxidation processes vary linearly with the square root of scan rates. (d) Plot of i_{cat}/i_d vs $\nu^{-1/2}$ with a slope of 1.12 $V^{1/2}$ $s^{-1/2}$. Conditions: ITO working electrode, 20 °C.

formation via a concerted O atom-proton transfer pathway.[58−60] This buffer anion effect was further supported by the CV of **1** in pH 7.0 acetate buffer (Figure 5a). CV comparison of **1** in phosphate, sulfate, and acetate solutions is significant, as it indicated that a formally Ni(IV) species could be the active catalytic species for water oxidation.

As shown in Figure 5b, the peak current of the first oxidation process in sulfate solution (in the absence of catalysis) varies linearly with the square root of scan rates, which is consistent with the Randles−Sevcik equation (eq 2).[11,39]

$$i_d = 0.4633nFAc_{cat}\sqrt{\frac{nF\upsilon D_{cat}}{RT}} \quad (2)$$

Here n = 1 is the number of electrons transferred in this process, and ν is the scan rate. The ratio of eq 1 to eq 2 gives eq 3

$$\frac{i_{cat}}{i_d} = 0.080\sqrt{\frac{k_{cat}T}{\upsilon}} \quad (3)$$

Here i_{cat}/i_d is consistent with the trend from pure diffusion behavior to pure kinetic behavior as scan rates decrease. With the molecular catalysis of **1** established, according to eq 3, the TOF value of 0.67 s^{-1} at room temperature can be determined from the slope of the linear plot of i_{cat}/i_d versus $\nu^{-1/2}$ in Figure 5d. It is worth noting that, as water oxidation is complicated, the calculated TOF is only an estimation of the catalytic performance.[11,61]

Similar to its Co porphyrin analogues, an inhibition effect was also observed with **1** at high phosphate concentrations. As shown in Figure 6, if the concentration of **1** was kept constant at 0.50 mM, the catalytic current initially increased rapidly and considerably with the increase of phosphate concentration up to 33 mM (Figure 6a), which was due to the phosphate-assisted O−O bond formation. In the range of 35−65 mM phosphate concentration, the change of catalytic currents was insignificant, and further increase of phosphate concentration caused the decrease of the catalytic currents (Figure 6b).

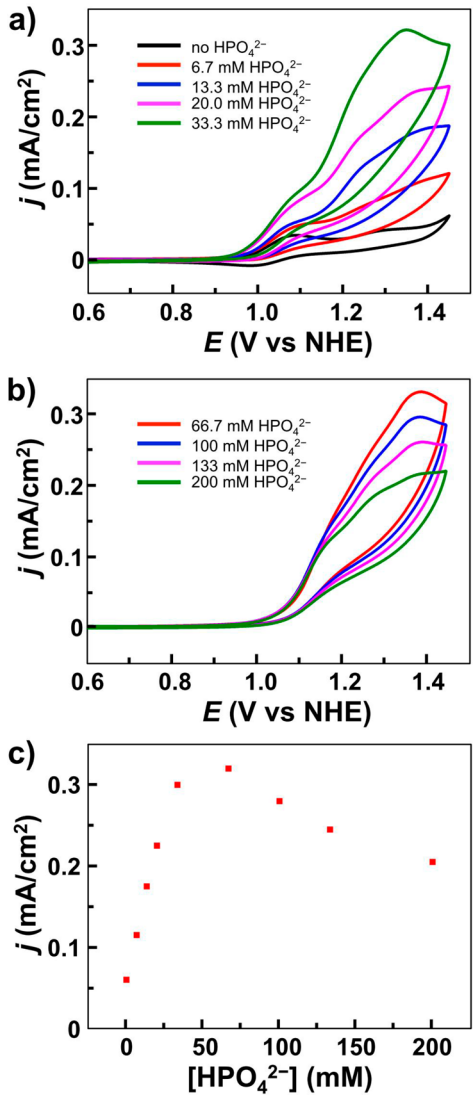

Figure 6. CVs of 0.50 mM of **1** in phosphate buffer at pH 7.0 with different phosphate concentrations. The ionic strength was maintained as constant with addition of sodium sulfate during these measurements. (a) The catalytic current increased rapidly with the increase of phosphate concentration. (b) The catalytic current decreased with further increase of phosphate concentration. (c) Plot of catalytic current at E = 1.32 V vs $[HPO_4^{2-}]$. Conditions: ITO working electrode, scan rate 50 mV s^{-1}, 20 °C.

These results from inhibition experiments can be summarized in Figure 6c, which shows a maximum catalytic current at a phosphate concentration of ca. 67 mM. It is necessary to mention that the ionic strength was maintained as constant during these measurements with addition of sodium sulfate. Wang and Groves studied this inhibition and proposed that it was caused by the coordination of phosphate anions on the metal center, which prevented the binding and therefore activation of water on the metal center.[13] This anion-assisted O−O bond formation step and buffer inhibition at high phosphate concentration are consistent with homogeneous catalysis.[13,58] In addition, such competitive coordination-caused inhibition was verified by inhibition experiments with acetonitrile. As shown in the electronic absorption spectra of **1** (Supporting Information Figure S17), the absorbance at 420 nm increased, while the shoulder at 445 nm decreased with an

DOI: 10.1021/acs.inorgchem.5b00924
Inorg. Chem. 2015, 54, 5604−5613

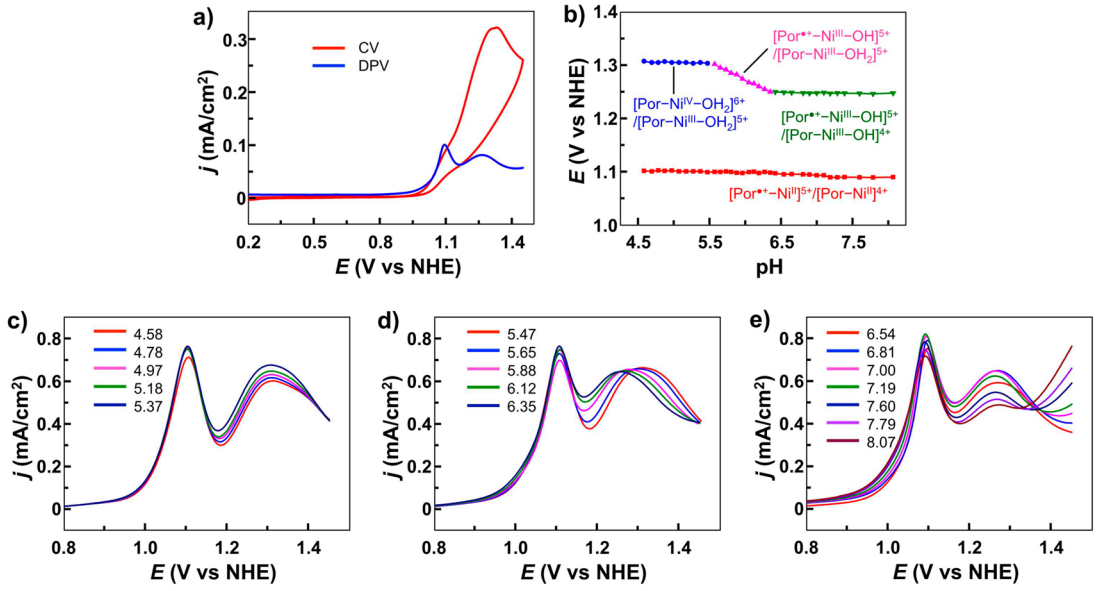

Figure 7. (a) CV and DPV of **1** in 0.10 M pH 7.0 phosphate buffer. (b) Dependence of the first and second oxidation peak potentials of **1** on pH from 4.58 to 8.07. DPVs of **1** in 0.10 M phosphate buffers with various pH values: (c) from 4.58 to 5.37, (d) from 5.47 to 6.35, (e) from 6.54 to 8.07. Conditions: ITO working electrode, 20 °C. DPV experimental parameters: increase potential, 0.004 V; amplitude, 0.05 V; pulse width, 0.05 s; sampling width, 0.0167 s; sample period, 0.5 s.

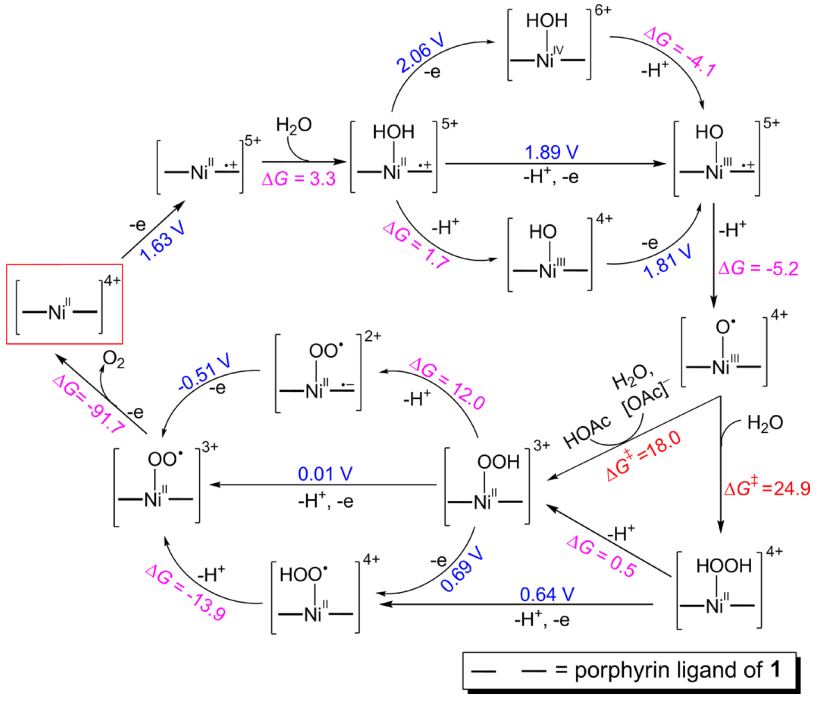

Figure 8. Proposed catalytic cycle for water oxidation with **1**.

isosbestic point at 431 nm upon addition of acetonitrile. This result suggested the coordination of acetonitrile at the Ni(II) site of **1**. Along with this change in UV–vis, the CV of **1** showed obvious inhibition in catalysis in the presence of acetonitrile (Supporting Information Figure S16), which proved that competitive coordination at the Ni(II) site could inhibit the water oxidation catalysis.

Kinetic isotope effect experiments were carried out, and a KIE value of 1.55 was obtained from the CVs of **1** recorded in D_2O and H_2O phosphate buffers under identical conditions (the KIE value was calculated according to KIE = $k_{cat,H_2O}/k_{cat,D_2O} = (i_{cat,H_2O}/i_{cat,D_2O})^2$, Supporting Information Figure S18). This result is consistent with a rate-limiting O–O bond formation step. As we addressed above, careful analysis of CVs of **1** in sulfate, acetate, and phosphate solutions suggested that water oxidation could be realized via a two-electron oxidized **1** (Figure 5a). In order to further investigate the redox process of **1** in phosphate buffer, differential pulse voltammetry (DPV) was used because of its higher sensitivity compared to CV and its ability to probe the redox processes under catalytic conditions.[62] The DPV of **1** displayed two oxidation waves at E_{pa} = 1.09 V and E_{pa} = 1.25 V in pH 7.0 phosphate buffer

DOI: 10.1021/acs.inorgchem.5b00924
Inorg. Chem. 2015, 54, 5604–5613

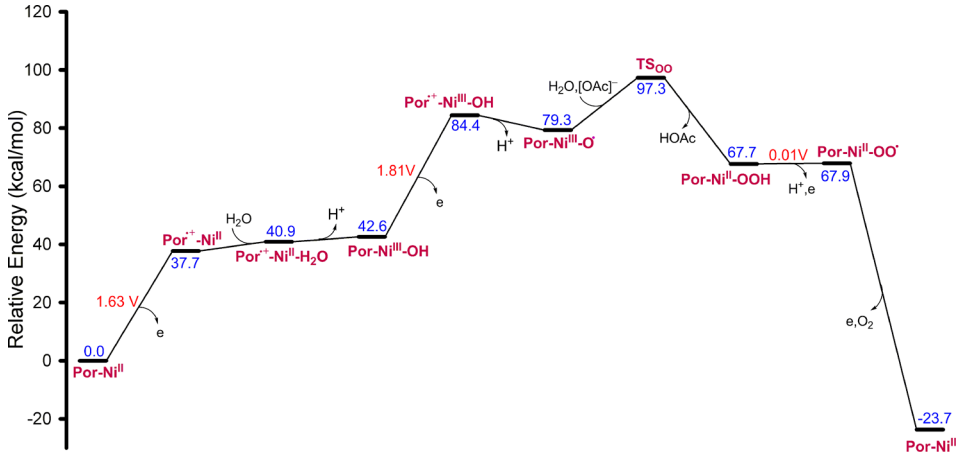

Figure 9. Energy diagram for water oxidation catalyzed by complex **1**. TS_{OO} is the TS of the base-assisted WNA reaction (see Figure 10b for its structure).

(Figure 7a), which were in excellent agreement with the two oxidation events observed in the CV of **1** in sulfate solution ($E_{1/2}$ = 1.07 V and E_{pa} = 1.29 V). The results from both CV and DPV measurements suggested that a formally Ni(IV) species generated by two one-electron oxidations of **1** was able to oxidize water.

In order to illuminate the water oxidation mechanism with **1**, DPVs were carried out in 0.1 M phosphate buffers with different pH values. As shown in Figure 7b–e, the first oxidation peak potential of **1** stayed almost unchanged in the pH range 4.58–8.07. For the second oxidation process, it is pH-dependent in the pH range 5.37–6.54, and the plot of the oxidation peak potential versus pH exhibited a linear dependence with a slope of −55 mV per pH unit, which indicated a $1H^+/1e^-$ procedure. However, the second oxidation exhibited pH-independence in the pH range 4.58–5.37 (E_{pa} = 1.31 V) and in the pH range 6.54–8.07 (E_{pa} = 1.25 V). Detailed parameters for DPV measurements are summarized in Figure 7.

The oxidation of water to generate hydrogen peroxide (H_2O_2) was not likely with **1** under our experimental conditions. First, our CPE and O_2 evolution experiments were carried out at 1.32 V in pH 7.0 phosphate buffer. Under this condition, water could not be oxidized to H_2O_2 from a thermodynamic point of view ($2H_2O \rightarrow H_2O_2 + 2H^+ + 2e^-$, E^θ = 1.78 V; at pH = 7.0, it is 1.37 V).[63] Second, no H_2O_2 was detected in the aqueous solution of **1** after 10 h of CPE by using an established method.[64] Furthermore, electrochemical measurements of **1** at rotating ring (Pt)-disk (GC) electrodes showed that no H_2O_2 was produced during the oxidation of water. The results from linear sweep voltammetry (LSV) of disk electrode with a scan rate of 10 mV s^{-1} and CPE of ring electrode at 0.70 V were shown in Supporting Information Figure S12. On the basis of these results, no current was observed at ring electrode due to the oxidation of H_2O_2.[53,54] The small current change on the ring electrode was due to the reduction of oxidized species of **1** at the ring electrode.

Computational Studies. Density functional theory (DFT) calculations were carried out to better understand the mechanism of water oxidation with **1**. The single crystal X-ray structure of the cationic Ni porphyrin (Por) unit of **1** was used as the starting point for geometry optimization. On the basis of our results, the catalytic cycle for water oxidation with **1** was proposed in Figure 8. The energy profile was summarized in Figure 9. The calculated potential for the first oxidation of **1** is 1.63 V, which corresponds to the oxidation of $[Por{-}Ni^{II}]^{4+}$ to $[Por^{\bullet+}{-}Ni^{II}]^{5+}$. This result is consistent with the fact that the first oxidation peak potential is independent of pH. Subsequent coordination of a water molecule on Ni atom of $[Por^{\bullet+}{-}Ni^{II}]^{5+}$ gives $[Por^{\bullet+}{-}Ni^{II}{-}OH_2]^{5+}$. The further one-electron oxidation of $[Por^{\bullet+}{-}Ni^{II}{-}OH_2]^{5+}$ gives $[Por^{\bullet+}{-}Ni^{III}{-}OH]^{5+}$, which has three different pathways, namely, electron transfer followed by proton transfer (ETPT), proton transfer followed by electron transfer (PTET), and proton-coupled electron transfer (PCET). The calculated oxidation potentials at pH 7.0 are 1.89 and 1.81 V for the $[Por^{\bullet+}{-}Ni^{II}{-}OH_2]^{5+}/[Por^{\bullet+}{-}Ni^{III}{-}OH]^{5+}$ and $[Por{-}Ni^{III}{-}OH]^{4+}/[Por^{\bullet+}{-}Ni^{III}{-}OH]^{5+}$ couples, respectively. The pH-dependence of the second oxidation in the pH range 5.37–6.54 suggested a PCET process. At pH 7.0, the second oxidation peak was assigned to the redox couple of $[Por{-}Ni^{III}{-}OH]^{4+}/[Por^{\bullet+}{-}Ni^{III}{-}OH]^{5+}$ due to its pH-independence in the pH range 6.54–8.07. Significantly, the calculated separation between the first and second oxidation of **1** at pH 7.0 is 0.18 V, which agrees very well with the value of 0.16 V from experimental DPV measurements.

It should be noted that, in our calculations, counteranions were omitted for simplicity. It is known that the nature and concentration of counteranions have substantial effects on the redox potential of positively charged nickel porphyrin species.[65] We tried to include counteranions in the calculation and found that, with addition of four OTf^- anions (the position of the OTf^- anions were determined from the X-ray structure of $\mathbf{1}(OTf)_4$), the calculated potential for the first oxidation of **1** was 1.48 V. Although this value is 0.15 V lower than that without counteranions, it is still larger than the experimental value. Given the challenges of accurate prediction of redox potentials using DFT methods,[40] the calculated redox potential separation is more meaningful. As we discussed above, our calculated separation between the first and second oxidation of **1** is in excellent agreement with the experimental value.

After two one-electron oxidation steps, the release of one proton from $[Por^{\bullet+}{-}Ni^{III}{-}OH]^{5+}$ occurred to give $[Por{-}Ni^{III}{-}O^{\bullet}]^{4+}$, which subsequently reacted with a water molecule to form the O–O bond via a concerted O atom-proton transfer pathway. Since previous studies suggested that the first and perhaps other solvation shells may play a decisive role in proton transfer as part of the O–O bond formation step,[66−74] we therefore investigated the water nucleophilic attack (WNA) reaction by including a cluster of four water molecules. We

DOI: 10.1021/acs.inorgchem.5b00924
Inorg. Chem. 2015, 54, 5604–5613

found that the O−O bond formation is concerted with a proton transfer process, in which one proton from the attacking water molecule transferred to the Ni-bounded O atom via the water cluster, leading to $[Por{-}Ni^{II}{-}HOOH]^{4+}$. This reaction was found to have an energy barrier of 24.9 kcal mol^{-1}. The transition state (TS) was showed in Figure 10a. On the other hand, we also studied the WNA reaction in the presence of an external base to investigate the possible base-assisted mechanism. Due to a large self-interaction error, the calculation with inclusion of a phosphate ion as an external base was not successful, as we also found in previous study of WNA reaction of a cobalt corrole system.[36] Alternatively, an acetate anion was used as an added base in our calculations. The located TS structure shows an increased O−O bond length (2.15 vs 1.96 Å, Figure 10), indicating a much earlier TS, as compared to that for $[Por{-}Ni^{III}{-}O^{\bullet}]^{4+}$ with four water molecules. The calculated energy barrier of 18.0 kcal mol^{-1} is significantly lower than that for $[Por{-}Ni^{III}{-}O^{\bullet}]^{4+}$ with four water molecules. In addition, the calculated H_2O/D_2O KIE value is 1.44. As shown in Figure 8, the base-assisted WNA reaction leads to the formation of $[Por{-}Ni^{II}{-}OOH]^{3+}$. A subsequent PCET reaction generates $[Por{-}Ni^{II}{-}OO^{\bullet}]^{3+}$ at a potential of 0.01 V. The further one-electron oxidation of $[Por{-}Ni^{II}{-}OO^{\bullet}]^{3+}$ results in the regeneration of **1** and the release of O_2 simultaneously.

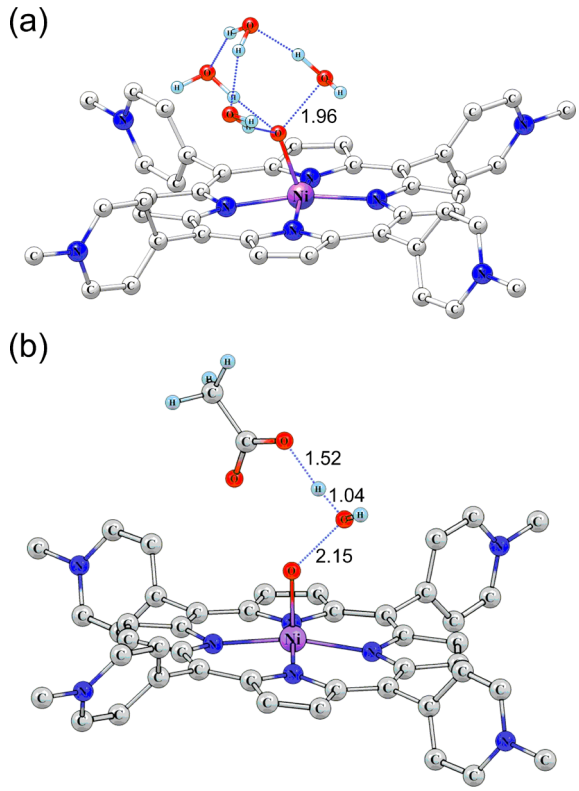

Figure 10. Transition state structure of O−O bond formation step via water nucleophilic attack. (a) $[Por{-}Ni^{III}{-}O^{\bullet}]^{4+}$ with four water molecules and (b) $[Por{-}Ni^{III}{-}O^{\bullet}]^{4+}$ in the presence of one water molecule and one OAc^{-} anion. The hydrogen atoms in the porphyrin ring were not shown for clarity.

Our calculations demonstrated that water oxidation with **1** via water nucleophilic attack to $[Por{-}Ni^{III}{-}O^{\bullet}]^{4+}$ is feasible. The O−O bond formation step was suggested to be the rate-limiting step in electrocatalytic water oxidation with **1**. It is interesting to compare the catalytic mechanism of Ni porphyrin and its Co porphyrin analogues. For Co porphyrin, Wang and Groves proposed that a formally Co(V) porphyrin is the active catalytic species for water oxidation,[13] but for Ni porphyrin, a formally Ni(IV) porphyrin, $[Por{-}Ni^{III}{-}O^{\bullet}]^{4+}$, is suggested to be able to oxidize water, which caused the onset of catalytic wave for water oxidation with **1** to lower by ∼200 mV as compared to its Co porphyrin analogues. This improvement was likely due to the fact that the redox potential of high-valent Ni atoms is considerably higher than that of Co in the same valence state.

CONCLUSION

As NiO_x is known to be highly active for water oxidation, great care has been made to ensure that **1** is the real molecular catalyst. Several lines of evidence have been provided in our work, including the following: (1) catalyst **1** is active in neutral and even acidic solutions; (2) **1** has different electrochemical behaviors in neutral vs basic solutions, and NiO_x films produced in basic solution of **1** are unstable at pH 7.0 under catalytic conditions; (3) there is no crossover, which is typical for metal oxide film deposition and catalysis, in the CV of **1**; (4) catalytic current has a linear relationship with the concentration of **1**; (5) free Ni(II) ions display no catalytic activity under identical conditions; (6) no current increase is observed in successive cycles of CVs and in CPE; (7) UV−vis shows almost identical spectra during and after 10 h of CPE; (8) the working electrode after CPE displays no catalytic current in a buffer-only solution, and no sign of any heterogeneous Ni phase is observed on the electrode as inspected by SEM and EDX or in the solution by Tyndall scattering analysis; (9) buffer and acetonitrile inhibition observed with **1** are consistent with a homogeneous, single-site water oxidation.

In summary, the water-soluble cationic nickel(II) porphyrin **1** was synthesized and examined as a single-site OER catalyst. Our results confirmed that **1** was able to electrocatalyze water oxidation to O_2 at neutral pH with low onset potential at ∼1.0 V. Mechanism studies revealed that the oxidation of water by a two-electron oxidized **1** is feasible. The onset of the catalytic wave for water oxidation with **1** is ∼200 mV lower compared to its Co porphyrin analogues and is the lowest among existing molecular OER catalysts in neutral aqueous solutions. Although the TOF of 0.67 s^{-1} is moderate, the verification of a single-site Ni-based molecular OER catalyst, low overpotential, homogeneous catalysis in neutral aqueous solutions, and catalyst stability are notable.

EXPERIMENTAL SECTION

General Materials and Methods. All reagents were purchased from commercial suppliers and used as received unless otherwise noted. Deionized water was used in all experiments. Porphyrins and nickel(II) porphyrins were prepared according to modified literature procedures.[75] ^1H NMR spectra were acquired on a Brüker spectrometer operating at 400 MHz. High-resolution mass spectrometric measurements were made on a Brüker Fourier transform ion cyclotron resonance mass spectrometer APEX IV at Peking University. Electronic absorption spectra were acquired on a Cary 50 spectrophotometer. The morphologies of the ITO surface before and after electrolysis were examined using a JSM-6700F field emission scanning electron microscope (FE-SEM). The EDX spectra were collected from three randomly selected areas of each sample. In addition, the materials were analyzed at several local spots to ensure their chemical homogeneity. Images were obtained with an acceleration voltage of 5 or 10 kV.

DOI: 10.1021/acs.inorgchem.5b00924
Inorg. Chem. 2015, 54, 5604−5613

Syntheses. *Tetrakis(4-pyridyl)porphyrin.* Freshly distilled pyrrole (5.04 g, 75 mmol) and 4-pyridinecarboxaldehyde (8.04 g, 75 mmol) were dissolved in propionic acid (150 mL), and the resulting solution was refluxed at 140 °C for 1.5 h in the dark. After the solvent was removed under reduced pressure, the residue was redissolved in DMF (220 mL) and was refluxed for 30 min. After being cooled to room temperature, the mixture was kept at −20 °C overnight during which time the porphyrin precipitated. The precipitate was filtered off, and the solid residue was carefully washed with ether following being dried under vacuum to give 1.77 g of purple solid (2.9 mmol, yield 15%).

Tetrakis(4-N-methylpyridyl)porphyrin Tetratosylate. Tetrakis(4-pyridyl)porphyrin (1.24 g, 2.0 mmol) and methyl tosylate (18.6 g, 100 mmol) were added into DMF (200 mL), and the resulting solution was refluxed for 16 h in the dark. The volume of DMF was reduced to ∼10 mL in vacuum, and the porphyrin was precipitated by addition of acetone (200 mL). The precipitate was filtered off and redissolved in water (200 mL). The aqueous phase washed by CH_2Cl_2 (200 mL × 3) was reduced to ∼10 mL. The porphyrin was precipitated again by addition of acetone (200 mL), and the precipitate was filtered off and dried under vacuum to give 2.04 g of purple solid (1.50 mmol, 75%). ^{1}H NMR (400 MHz, DMSO-d_6): δ 9.49 (d, J = 6.3 Hz, 8H), 9.19 (s, 8H), 8.98 (d, J = 6.4 Hz, 8H), 7.46 (d, J = 7.9 Hz, 8H), 7.05 (d, J = 7.9 Hz, 8H), 4.73 (s, 12H), 2.22 (s, 12H), −3.10 (s, 2H).

Nickel(II) Tetrakis(4-N-methylpyridyl)porphyrin Tetrahexafluorophosphate (1(PF$_6$)$_4$). Tetrakis(4-*N*-methylpyridyl)porphyrin tetratosylate (682 mg, 0.50 mmol) and $Ni(OAc)_2{\cdot}4H_2O$ (871 mg, 3.5 mmol) were added into DMF/H_2O (1:1, 30 mL), and then the resulting solution was heated at 100 °C for 6 h in the dark. After being cooled to room temperature, the residue from removing the solvents under reduced pressure was dissolved in water (200 mL). Nickel(II) porphyrin was precipitated by addition of a saturated aqueous NH_4PF_6 solution (ca. 50 mL), and then the precipitate was filtered off, washed with ether, and dried in vacuum to yield 0.56 g of red solid (0.43 mmol, 85%). Red needle-like crystals of $\mathbf{1}(PF_6)_4$ were obtained by slow evaporation from CH_3CN and H_2O solution at room temperature. High-resolution ESI-MS for $[Ni^{II}(C_{44}H_{36}N_8)(PF_6)_2]^{2+}$: calcd 512.0850; found 512.0845.

Nickel(II) Tetrakis(4-N-methylpyridyl)porphyrin Tetratriflate (1(OTf)$_4$). The red needle-like crystals of $\mathbf{1}(PF_6)_4$ were taken in a mixture of CH_3CN/H_2O (1:1), and PF_6^- anions were exchanged by OTf^- on anion exchange resin by slow stirring at ambient temperature for 48 h. The solution was filtered, and the resin was washed with methanol. The solvents were removed under reduced pressure to give a red solid. Red needle-like crystals of $\mathbf{1}(OTf)_4$ were obtained by slow evaporation from CH_3OH and H_2O at room temperature. ^{1}H NMR (400 MHz, CD_3CN): δ 9.07 (d, J = 6.3 Hz, 8H), 9.02 (s, 8H), 8.67 (d, J = 6.3 Hz, 8H), 4.66 (s, 12H) (Supporting Information Figure S3).

Crystallographic Studies. The complete data sets for red needle-like crystals of $\mathbf{1}(PF_6)_4$ and $\mathbf{1}(OTf)_4$ were collected. Single crystals suitable for X-ray analysis were each coated with Paratone-N oil, suspended in a small fiber loop, and placed in a cooled gas stream at 150(2) K on a Bruker D8 Venture X-ray diffractometer. Diffraction intensities were measured using graphite monochromated Mo Kα radiation (λ = 0.710 73 Å). Data collection, indexing, data reduction, and final unit cell refinements were carried out using APEX2;[76] absorption corrections were applied using the program SADABS.[77] The structure was solved by direct methods using SHELXS[78] and refined against F^2 on all data by full-matrix least-squares with SHELXL,[79] following established refinement strategies. Crystallographic studies revealed that both $\mathbf{1}(PF6)_4$ and $\mathbf{1}(OTf)_4$ crystallized in the monoclinic space group $C2/c$. All non-hydrogen atoms were refined anisotropically. All hydrogen atoms binding to carbon were included in the model at geometrically calculated positions and refined using a riding model. The isotropic displacement parameters of all hydrogen atoms were fixed to 1.2 times the U value of the atoms they are linked to (1.5 times for methyl groups). The CIF of $\mathbf{1}(OTf)_4$ contains level B alerts (isolated oxygen atom for O1S and O2S). Atoms O1S and O2S are oxygen atoms of cocrystallized solvent water molecules. Due to the positional disorder of the hydrogen atoms of solvent water molecules, we did not include them in the refinement. Details of the data quality and a summary of the residual values of the refinements are listed in Supporting Information Table S1.

Electrochemical Studies. All electrochemical experiments were carried out using a CH Instruments (model CHI660E electrochemical analyzer) at 20 °C unless otherwise noted. Cyclic voltammograms (CVs) and differential pulse voltammetries (DPVs) were performed in 6 mL of aqueous solutions and used a three-compartment cell with a 0.25 cm^2 tin-doped indium oxide (ITO) electrode as the working electrode, saturated Ag/AgCl as the reference electrode, and Pt wire as the auxiliary electrode. All potentials are reported versus the normal hydrogen electrode (NHE) through the addition of 0.199 V to the measured potentials. The working electrode was ultrasonically washed with deionized water. Constant potential electrolysis recorded in 15 mL of 0.10 M pH 7.0 phosphate buffer containing 0.75 mM of $\mathbf{1}(OTf)_4$ was carried out at 1.32 V in a fritted cell with a 2.0 cm^2 ITO working electrode.

The possible H_2O_2 formation was examined by electrochemical measurements using rotating ring-disk electrode. Electrochemistry of **1** was conducted at a rotating ring (Pt)-disk (GC) electrode in 0.10 M of pH 7.0 phosphate buffer. Linear sweep voltammetry (LSV) of the disk electrode with a scan rate of 10 mV s^{-1} and CPE of the ring electrode at 0.70 V were shown in Supporting Information Figure S12. The results showed that no oxidation of H_2O_2 was observed at the ring electrode, and the decline of ring current was due to the reduction of oxidized species of **1** at the ring electrode.

Characterization of Oxygen Evolution. CPE of 0.75 mM of **1** in 15 mL of 0.10 M pH 7.0 phosphate buffer was carried out at 1.32 V in a three-compartment gastight electrochemical cell with a Schlenk connection on each compartment (Supporting Information Figure S19). One compartment contained a Pt auxiliary electrode, one contained the 2.0 cm^2 ITO working electrode, and one contained the Ag/AgCl reference electrode. Analysis of O_2 produced in CPE experiments was conducted by using a calibrated Ocean Optics FOXY probe (Model NeoFox) which was immersed into the solution having the ITO working electrode. The solution was bubbled with argon for 1 h with vigorous stirring to remove O_2. The phase shift of the O_2 sensor on the FOXY probe, recorded at 10 s intervals, was converted into the concentration of O_2 in the solution using a two-point calibration curve (air, 20.9% O_2; high purity argon, 0% O_2). Background from the buffer-only solution was measured in the same method and was deducted.

Theoretical Methods. All calculations were done with density functional theory (DFT) as implemented in the Gaussian 09 software package.[80] Optimization and frequency calculations were performed using the B3LYP functional in combination with the def-SVP basis set.[81] The energy was then corrected by using a larger basis set, def-TZVP.[82] All optimizations and single point calculations were performed with solvation included using conductor-like polarizable continuum model (CPCM)[83] in water. For redox potential calculations, reference potential of normal hydrogen electrode (NHE) was set at −4.28 eV,[36,84] and the standard free energy of proton was set at −272.2 kcal mol^{-1}.[36] The H_2O/D_2O KIE for the base-assisted WNA reaction was calculated using Gaussian frequency data based on the semiclassical Eyring equation[85]

$$\frac{k_H}{k_D} = \exp\left[-\frac{(G_H^{\#} - G_H^{R}) - (G_D^{\#} - G_D^{R})}{RT}\right]$$

where G is the Gibbs free energy, superscript R denotes reagent, and # represents TS.

■ ASSOCIATED CONTENT

Supporting Information

Figures S1−S19, Table S1, crystallographic data in CIF format for $\mathbf{1}(OTf)_4$ and $\mathbf{1}(PF_6)_4$, and Cartesian coordinates of DFT-optimized structures. The Supporting Information is available free of charge on the ACS Publications website at DOI: 10.1021/acs.inorgchem.5b00924.

DOI: 10.1021/acs.inorgchem.5b00924
Inorg. Chem. 2015, 54, 5604−5613

AUTHOR INFORMATION

Corresponding Authors

*E-mail: wenzhenlai@ruc.edu.cn.

*E-mail: ruicao@ruc.edu.cn.

Notes

The authors declare no competing financial interest.

ACKNOWLEDGMENTS

We thank Prof. Ming-Tian Zhang and Xiao-Jun Su for helpful discussions and assistance in O_2 detection. We are grateful to the support from the "Thousand Talents Program" in China, the National Natural Science Foundation of China under Grants 21101170 and 21203245, the Fundamental Research Funds for the Central Universities, and the Research Funds of Renmin University of China.

REFERENCES

(1) Concepcion, J. J.; Jurss, J. W.; Brennaman, M. K.; Hoertz, P. G.; Patrocinio, A. O. T.; Iha, N. Y. M.; Templeton, J. L.; Meyer, T. J. *Acc. Chem. Res.* **2009**, *42*, 1954−1965.

(2) Dau, H.; Zaharieva, I. *Acc. Chem. Res.* **2009**, *42*, 1861−1870.

(3) Nocera, D. G. *Acc. Chem. Res.* **2012**, *45*, 767−776.

(4) Ferreira, K. N.; Iverson, T. M.; Maghlaoui, K.; Barber, J.; Iwata, S. *Science* **2004**, *303*, 1831−1838.

(5) Loll, B.; Kern, J.; Saenger, W.; Zouni, A.; Biesiadka, J. *Nature* **2005**, *438*, 1040−1044.

(6) Kohl, S. W.; Weiner, L.; Schwartsburd, L.; Konstantinovski, L.; Shimon, L. J. W.; Ben-David, Y.; Iron, M. A.; Milstein, D. *Science* **2009**, *324*, 74−77.

(7) Eisenberg, R. *Science* **2009**, *324*, 44−45.

(8) Kanan, M. W.; Nocera, D. G. *Science* **2008**, *321*, 1072−1075.

(9) Smith, R. D. L.; Prévot, M. S.; Fagan, R. D.; Zhang, Z. P.; Sedach, P. A.; Siu, M. K. J.; Trudel, S.; Berlinguette, C. P. *Science* **2013**, *340*, 60−63.

(10) Dincă, M.; Surendranath, Y.; Nocera, D. G. *Proc. Natl. Acad. Sci. U.S.A.* **2010**, *107*, 10337−10341.

(11) Barnett, S. M.; Goldberg, K. I.; Mayer, J. M. *Nat. Chem.* **2012**, *4*, 498−502.

(12) Bediako, D. K.; Costentin, C.; Jones, E. C.; Nocera, D. G.; Savéant, J. M. *J. Am. Chem. Soc.* **2013**, *135*, 10492−10502.

(13) Wang, D.; Groves, J. T. *Proc. Natl. Acad. Sci. U.S.A.* **2013**, *110*, 15579−15584.

(14) Zong, R. F.; Thummel, R. P. *J. Am. Chem. Soc.* **2005**, *127*, 12802−12803.

(15) Wasylenko, D. J.; Ganesamoorthy, C.; Henderson, M. A.; Koivisto, B. D.; Osthoff, H. D.; Berlinguette, C. P. *J. Am. Chem. Soc.* **2010**, *132*, 16094−16106.

(16) Concepcion, J. J.; Jurss, J. W.; Templeton, J. L.; Meyer, T. J. *J. Am. Chem. Soc.* **2008**, *130*, 16462−16463.

(17) Chen, Z. F.; Concepcion, J. J.; Jurss, J. W.; Meyer, T. J. *J. Am. Chem. Soc.* **2009**, *131*, 15580−15581.

(18) Concepcion, J. J.; Tsai, M. K.; Muckerman, J. T.; Meyer, T. J. *J. Am. Chem. Soc.* **2010**, *132*, 1545−1557.

(19) Duan, L. L.; Fischer, A.; Xu, Y. H.; Sun, L. C. *J. Am. Chem. Soc.* **2009**, *131*, 10397−10399.

(20) Duan, L. L.; Bozoglian, F.; Mandal, S.; Stewart, B.; Privalov, T.; Llobet, A.; Sun, L. C. *Nat. Chem.* **2012**, *4*, 418−423.

(21) McDaniel, N. D.; Coughlin, F. J.; Tinker, L. L.; Bernhard, S. *J. Am. Chem. Soc.* **2008**, *130*, 210−217.

(22) Cao, R.; Ma, H. Y.; Geletii, Y. V.; Hardcastle, K. I.; Hill, C. L. *Inorg. Chem.* **2009**, *48*, 5596−5598.

(23) Hull, J. F.; Balcells, D.; Blakemore, J. D.; Incarvito, C. D.; Eisenstein, O.; Brudvig, G. W.; Crabtree, R. H. *J. Am. Chem. Soc.* **2009**, *131*, 8730−8731.

(24) Blakemore, J. D.; Schley, N. D.; Balcells, D.; Hull, J. F.; Olack, G. W.; Incarvito, C. D.; Eisenstein, O.; Brudvig, G. W.; Crabtree, R. H. *J. Am. Chem. Soc.* **2010**, *132*, 16017−16029.

(25) Moore, G. F.; Blakemore, J. D.; Milot, R. L.; Hull, J. F.; Song, H. E.; Cai, L.; Schmuttenmaer, C. A.; Crabtree, R. H.; Brudvig, G. W. *Energy Environ. Sci.* **2011**, *4*, 2389−2392.

(26) Santoni, M. P.; La Ganga, G.; Nardo, V. M.; Natali, M.; Puntoriero, F.; Scandola, F.; Campagna, S. *J. Am. Chem. Soc.* **2014**, *136*, 8189−8192.

(27) Shimazaki, Y.; Nagano, T.; Takesue, H.; Ye, B. H.; Tani, F.; Naruta, Y. *Angew. Chem., Int. Ed.* **2004**, *43*, 98−100.

(28) Ellis, W. C.; McDaniel, N. D.; Bernhard, S.; Collins, T. J. *J. Am. Chem. Soc.* **2010**, *132*, 10990−10991.

(29) Fillol, J. L.; Codolà, Z.; Garcia-Bosch, I.; Gómez, L.; Pla, J. J.; Costas, M. *Nat. Chem.* **2011**, *3*, 807−813.

(30) Coggins, M. K.; Zhang, M.-T.; Vannucci, A. K.; Dares, C. J.; Meyer, T. J. *J. Am. Chem. Soc.* **2014**, *136*, 5531−5534.

(31) Wu, Y. Z.; Chen, M. X.; Han, Y. Z.; Luo, H. X.; Su, X. J.; Zhang, M.-T.; Lin, X. H.; Sun, J. L.; Wang, L.; Deng, L.; Zhang, W.; Cao, R. *Angew. Chem., Int. Ed.* **2015**, *54*, 4870−4875.

(32) Dogutan, D. K.; McGuire, R., Jr.; Nocera, D. G. *J. Am. Chem. Soc.* **2011**, *133*, 9178−9180.

(33) Gerken, J. B.; McAlpin, J. G.; Chen, J. Y. C.; Rigsby, M. L.; Casey, W. H.; Britt, R. D.; Stahl, S. S. *J. Am. Chem. Soc.* **2011**, *133*, 14431−14442.

(34) Wasylenko, D. J.; Ganesamoorthy, C.; Borau-Garcia, J.; Berlinguette, C. P. *Chem. Commun.* **2011**, *47*, 4249−4251.

(35) Nakazono, T.; Parent, A. R.; Sakai, K. *Chem. Commun.* **2013**, *49*, 6325−6327.

(36) Lei, H. T.; Han, A. L.; Li, F. W.; Zhang, M. N.; Han, Y. Z.; Du, P. W.; Lai, W. Z.; Cao, R. *Phys. Chem. Chem. Phys.* **2014**, *16*, 1883−1893.

(37) Chen, Z. F.; Meyer, T. J. *Angew. Chem., Int. Ed.* **2013**, *52*, 700−703.

(38) Chen, Z. F.; Rathmell, A. R.; Ye, S. R.; Wilson, A. R.; Wiley, B. J. *Angew. Chem., Int. Ed.* **2013**, *52*, 13708−13711.

(39) Zhang, M.-T.; Chen, Z. F.; Kang, P.; Meyer, T. J. *J. Am. Chem. Soc.* **2013**, *135*, 2048−2051.

(40) Zhang, T.; Wang, C.; Liu, S. B.; Wang, J. L.; Lin, W. B. *J. Am. Chem. Soc.* **2014**, *136*, 273−281.

(41) Coggins, M. K.; Zhang, M.-T.; Chen, Z. F.; Song, N.; Meyer, T. J. *Angew. Chem., Int. Ed.* **2014**, *53*, 12226−12230.

(42) Su, X.-J.; Gao, M.; Jiao, L.; Liao, R.-Z.; Siegbahn, P. E. M.; Cheng, J.-P.; Zhang, M.-T. *Angew. Chem., Int. Ed.* **2015**, *54*, 4909−4914.

(43) Cao, R.; Lai, W. Z.; Du, P. W. *Energy Environ. Sci.* **2012**, *5*, 8134−8157.

(44) Hetterscheid, D. G. H.; Reek, J. N. H. *Angew. Chem., Int. Ed.* **2012**, *51*, 9740−9747.

(45) Wasylenko, D. J.; Palmer, R. D.; Berlinguette, C. P. *Chem. Commun.* **2013**, *49*, 218−227.

(46) Dey, S.; Mondal, B.; Dey, A. *Phys. Chem. Chem. Phys.* **2014**, *16*, 12221−12227.

(47) Bediako, D. K.; Lassalle-Kaiser, B.; Surendranath, Y.; Yano, J.; Yachandra, V. K.; Nocera, D. G. *J. Am. Chem. Soc.* **2012**, *134*, 6801−6809.

(48) Singh, A.; Chang, S. L. Y.; Hocking, R. K.; Bach, U.; Spiccia, L. *Catal. Sci. Technol.* **2013**, *3*, 1725−1732.

(49) Singh, A.; Chang, S. L. Y.; Hocking, R. K.; Bach, U.; Spiccia, L. *Energy Environ. Sci.* **2013**, *6*, 579−586.

(50) Gao, M. R.; Sheng, W. C.; Zhuang, Z. B.; Fang, Q. R.; Gu, S.; Jiang, J.; Yan, Y. S. *J. Am. Chem. Soc.* **2014**, *136*, 7077−7084.

(51) Zhang, M.; Zhang, M.-T.; Hou, C.; Ke, Z. F.; Lu, T. B. *Angew. Chem., Int. Ed.* **2014**, *53*, 13042−13048.

(52) Collman, J. P.; Devaraj, N. K.; Decréau, R. A.; Yang, Y.; Yan, Y. L.; Ebina, W.; Eberspacher, T. A.; Chidsey, C. E. D. *Science* **2007**, *315*, 1565−1568.

(53) Wasylenko, D. J.; Rodríguez, C.; Pegis, M. L.; Mayer, J. M. *J. Am. Chem. Soc.* **2014**, *136*, 12544−12547.

(54) McGuire, R., Jr.; Dogutan, D. K.; Teets, T. S.; Suntivich, J.; Shao-Horn, Y.; Nocera, D. G. *Chem. Sci.* **2010**, *1*, 411−414.

DOI: 10.1021/acs.inorgchem.5b00924
Inorg. Chem. 2015, 54, 5604−5613

(55) Kleingardner, J. G.; Kandemir, B.; Bren, K. L. *J. Am. Chem. Soc.* **2014**, *136*, 4−7.
(56) Lee, C. H.; Dogutan, D. K.; Nocera, D. G. *J. Am. Chem. Soc.* **2011**, *133*, 8775−8777.
(57) Pasternack, R. F.; Sutin, N.; Turner, D. H. *J. Am. Chem. Soc.* **1976**, *98*, 1908−1913.
(58) Chen, Z. F.; Concepcion, J. J.; Hu, X. Q.; Yang, W. T.; Hoertz, P. G.; Meyer, T. J. *Proc. Natl. Acad. Sci. U.S.A.* **2010**, *107*, 7225−7229.
(59) Lai, W. Z.; Cao, R.; Dong, G.; Shaik, S.; Yao, J. N.; Chen, H. *J. Phys. Chem. Lett.* **2012**, *3*, 2315−2319.
(60) Baran, J. D.; Grönbeck, H.; Hellman, A. *J. Am. Chem. Soc.* **2014**, *136*, 1320−1326.
(61) Costentin, C.; Drouet, S.; Robert, M.; Savéant, J. M. *J. Am. Chem. Soc.* **2012**, *134*, 11235−11242.
(62) Bard, A. J.; Faulkner, L. R. *Electrochemical Methods*; Wiley: New York, 1980.
(63) Izgorodin, A.; Izgorodina, E.; MacFarlane, D. R. *Energy Environ. Sci.* **2012**, *5*, 9496−9501.
(64) Mittra, K.; Chatterjee, S.; Samanta, S.; Dey, A. *Inorg. Chem.* **2013**, *52*, 14317−14325.
(65) Kadish, K. M.; Lin, M.; Van Caemelbecke, E.; De Stefano, G.; Medforth, C. J.; Nurco, D. J.; Nelson, N. Y.; Krattinger, B.; Muzzi, C. M.; Jaquinod, L.; Xu, Y.; Shyr, D. C.; Smith, K. M.; Shelnutt, J. A. *Inorg. Chem.* **2002**, *41*, 6673−6687.
(66) Ertem, M. Z.; Gagliardi, L.; Cramer, C. J. *Chem. Sci.* **2012**, *3*, 1293−1299.
(67) Ertem, M. Z.; Cramer, C. J. *Dalton Trans.* **2012**, *41*, 12213−12219.
(68) Bozoglian, F.; Romain, S.; Ertem, M. Z.; Todorova, T. K.; Sens, C.; Mola, J.; Rodríguez, M.; Romero, I.; Benet-Buchholz, J.; Fontrodona, X.; Cramer, C. J.; Gagliardi, L.; Llobet, A. *J. Am. Chem. Soc.* **2009**, *131*, 15176−15187.
(69) Sartorel, A.; Miró, P.; Salvadori, E.; Romain, S.; Carraro, M.; Scorrano, G.; Di Valentin, M.; Llobet, A.; Bo, C.; Bonchio, M. *J. Am. Chem. Soc.* **2009**, *131*, 16051−16053.
(70) Sala, X.; Ertem, M. Z.; Vigara, L.; Todorova, T. K.; Chen, W. Z.; Rocha, R. C.; Aquilante, F.; Cramer, C. J.; Gagliardi, L.; Llobet, A. *Angew. Chem., Int. Ed.* **2010**, *49*, 7745−7747.
(71) Wang, L. P.; Wu, Q.; Van Voorhis, T. *Inorg. Chem.* **2010**, *49*, 4543−4553.
(72) Bianco, R.; Hay, P. J.; Hynes, J. T. *J. Phys. Chem. A* **2011**, *115*, 8003−8016.
(73) Li, X. C.; Chen, G. J.; Schinzel, S.; Siegbahn, P. E. M. *Dalton Trans.* **2011**, *40*, 11296−11307.
(74) Vigara, L.; Ertem, M. Z.; Planas, N.; Bozoglian, F.; Leidel, N.; Dau, H.; Haumann, M.; Gagliardi, L.; Cramer, C. J.; Llobet, A. *Chem. Sci.* **2012**, *3*, 2576−2586.
(75) Romera, C.; Sabater, L.; Garofalo, A.; Dixon, I. M.; Pratviel, G. *Inorg. Chem.* **2010**, *49*, 8558−8567.
(76) Bruker AXS. *APEX2 v2009*; Madison, WI, 2009.
(77) Sheldrick, G. M. *SADABS, 2008/1*; University of Göttingen: Göttingen, Germany, 2008.
(78) Sheldrick, G. M. *Acta Crystallogr.* **1990**, *A46*, 467−473.
(79) Sheldrick, G. M. *Acta Crystallogr.* **2008**, *A64*, 112−122.
(80) Frisch, M. J.; et al. *Gaussian 09, Revision C.01*, Gaussian, Inc.: Wallingford, CT, 2010.
(81) Schäfer, A.; Horn, H.; Ahlrichs, R. *J. Chem. Phys.* **1992**, *97*, 2571−2577.
(82) Schäfer, A.; Huber, C.; Ahlrichs, R. *J. Chem. Phys.* **1994**, *100*, 5829−5835.
(83) Barone, V.; Cossi, M. *J. Phys. Chem. A* **1998**, *102*, 1995−2001.
(84) Kelly, C. P.; Cramer, C. J.; Truhlar, D. G. *J. Phys. Chem. B* **2006**, *110*, 16066−16081.
(85) Wang, Y.; Kumar, D.; Yang, C. L.; Han, K. L.; Shaik, S. *J. Phys. Chem. B* **2007**, *111*, 7700−7710.

DOI: 10.1021/acs.inorgchem.5b00924
Inorg. Chem. 2015, 54, 5604−5613